

# Computational modeling of responses in human visual cortex

**Brian A. Wandell** <sup>1,2</sup>

**Jonathan Winawer** <sup>3</sup>

**Kendrick N. Kay** <sup>1,4</sup>

1. Psychology Department, Stanford University
2. Stanford's Center for Cognitive and Neurobiological Imaging
3. Psychology Department, New York University
4. Psychology Department, Washington University, St. Louis

Contact: [Wandell@stanford.edu](mailto:Wandell@stanford.edu)

“It's tough to make predictions, especially about the future”  
*(Attributed to Niels Bohr, Yogi Berra, and Mark Twain).*

## Related chapters

- 22. fMRI at high field - spatial resolution limits and applications
- 29. Visuomotor integration
- 34. Early visual processing
- 36. Visual object recognition
- 37. Face processing
- 163. Action Perception
- 224. Functional organization of the primary visual cortex
- 225. Higher visual cortex
- 358. Reading

## Glossary

- fMRI – functional magnetic resonance imaging
- ECoG – Electrocorticography (electrical recordings from intracranial electrodes)
- Visual field map (retinotopic map) – Spatial representation of the visual field within visual cortex
- Visual receptive field - The region of space in which the presence of a stimulus elicits a response
- Striate cortex – V1
- Extrastriate cortex – Visual cortex outside of V1, including V2, V3 and so forth
- Stimulus-referred – Experimental designs that characterize the neural response with respect to the stimulus properties

## Key Words

Neuroimaging, fMRI, ECoG, visual cortex, retinotopy, vision, receptive field, intracranial recording, visual field map, computational modeling, visual perception, contrast perception, extrastriate cortex, striate cortex

## Synopsis

A new generation of models and experimental designs are clarifying the computational principles in human visual cortex. Over the first two decades of functional magnetic resonance imaging, steady progress in measuring visual cortex led to the identification of more than twenty retinotopically mapped cortical areas. New models are being developed to predict responses in these maps and thus clarify their functional roles. Many of these models are based on a stimulus-referred approach, so that the computational principles can be tested using multiple types of measurements - spanning functional MRI, intracranial recordings, and single-unit measurements. The stimulus-referred approach promises to build an integrated view of neural computations measured across temporal and spatial scales.

## Introduction

Many fields of investigation, spanning medicine, science, and humanities, have an interest in the spatially localized measurements of human brain activity provided by functional magnetic resonance imaging (fMRI). These fields use a diverse array of experimental, statistical and computational methods to analyze and interpret fMRI responses, and this diversity reflects the questions of interest to each field.

The approach in vision science differs substantially from that taken in most other fields. Most disciplines use neuroimaging designs based on between-group or between-condition comparisons; the primary aim in these experiments is to find statistically significant group differences that localize function by combining weak signals. But the fMRI signals in visual

cortex are relatively strong, so that experiments can be performed in individual subjects using a wide range of stimuli. Further, the spatial organization and high degree of connectivity across visual cortex is clear, so that localization is not a driving factor. Instead, the principal goals of neuroimaging in vision science are (a) to develop computational models that predict the fMRI responses for a wide range of stimuli, and (b) to integrate neuroimaging measurements with data from other techniques (psychophysics, intracranial recordings, single-unit physiology, and so forth). To support these goals, neuroimaging designs for vision science use parametric variations of the stimulus and computational models that compute the mapping from stimuli to fMRI time series. In vision science, computational modeling is central and statistical analyses are secondary.

We illustrate and explain the approach in the following sections. First, we introduce visual field maps (also called retinotopic maps). This background section provides the reader with a sense of the cortical locations where we measure fMRI responses and the quality of the fMRI time series in visual cortex. Second, we describe the importance of stimulus-referred measurement in vision science. This approach is critical for integrating different types of measurements. Third, we describe the current generation of computational models of the fMRI time series. These models extend conventional visual field mapping and analyze the time series more fully. Finally, we illustrate how these models and stimulus-referred methods have clarified the relationship between fMRI and intracranial data obtained from human visual cortex.

## Visual field maps

In the mid-1800s, biologists began examining the responses in animal brains to localize various stimulus-driven responses. Visual cortex was localized rather early, though not without some serious disputes (1-3). The biologists were joined in the late 19<sup>th</sup> and early 20<sup>th</sup> centuries by neurologists and ophthalmologists (4-7). The clinicians treated soldiers who had occipital head wounds that caused blindness in restricted regions of the visual field. By mapping correspondences between the wound location and the visual field loss, Inouye, Holmes and others showed that the position of the wound corresponded to the location of the visual field loss. They correctly concluded that there is at least one topographic map of the contralateral visual hemifield in each hemisphere.

In the 1940s, electrophysiology in animal brains revealed that there are multiple sensory maps. It is challenging to measure visual field maps using single-unit electrophysiology. The experiment requires a series of electrode penetrations through the folded cortical sheet, followed by a histological reconstruction so that the electrode positions might be integrated with the responses. Hubel and Wiesel characterized the work as “a dismaying exercise in tedium, like trying to cut the back lawn with a pair of nail scissors (p. 28 (8)).” Even so, good progress was made, and by the early 1990s electrophysiologists and anatomists identified dozens of maps in various species (3, 9).

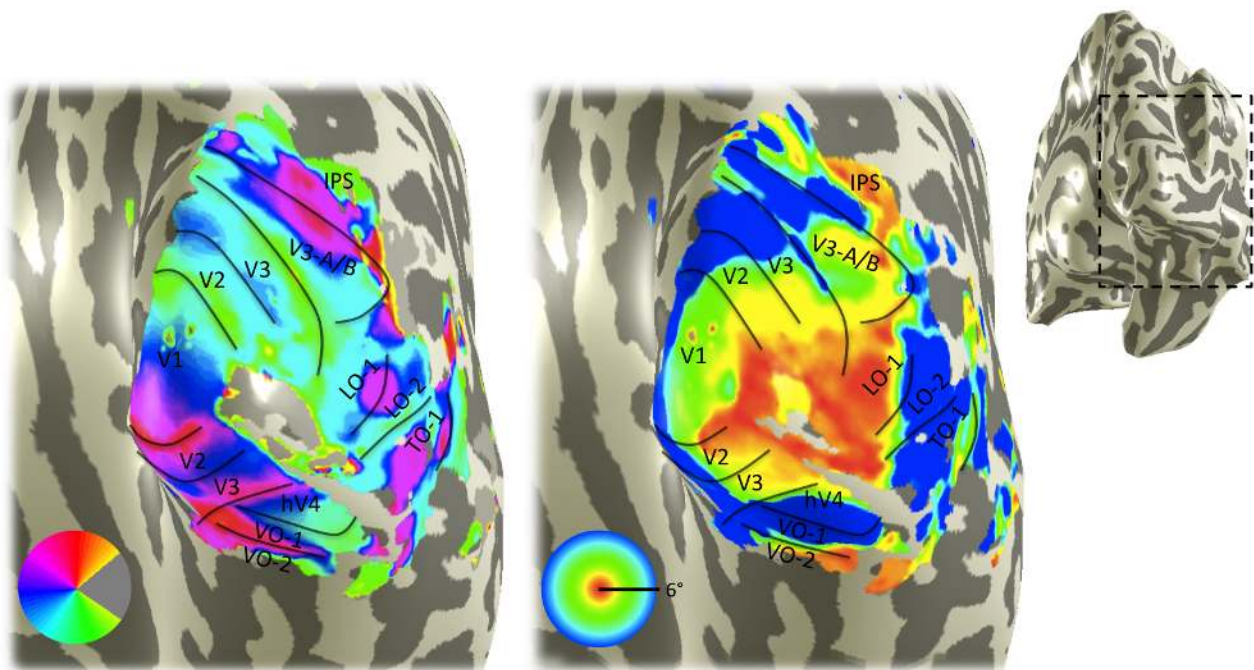


**Figure 1. Visual field maps in occipital cortex.** The small inset at the upper right is a smoothed rendering of the surface boundary between gray matter and white matter in a right hemisphere, and the dotted rectangle is shown in the magnified and further smoothed images. The dark and light gray shading indicates sulci and gyri, respectively. The two main images show visual cortex rendered from a point behind the occipital pole. The underlying anatomy is the same for the two meshes, differing only in the color overlays. The color overlays show the most effective angle (left) or the most effective eccentricity (right). Colors are shown only for voxels where the data are well fit by a population receptive field model, as explained below. The solid black lines and labels indicate the positions of ten visual field maps. The view and data were selected to provide a large field of view spanning most of the occipital lobe. Additional maps have been identified, including some on the intraparietal sulcus (IPS) and anterior ventral surface (10-14). The uncolored region on the ventral surface is close to a large sinus that limits the ability to measure the BOLD signal (15).

The first human fMRI experiments measured cortical responses to visual stimuli that covered a large part of the visual field (16, 17). These stimuli elicited responses in a broad swath of occipital cortex. Shortly thereafter, fMRI measurements clarified the relationship between stimulus visual field position and cortical responses (18-21). In one widely adopted method, the experimenter presents a contrast pattern within a series of concentric rings of, say, increasing inner and outer diameters (22). Such an expanding ring stimulus generates a traveling wave of activity that begins at the occipital pole when the ring diameter is small and travels to the peripheral representation as the ring diameter increases; these responses define the eccentricity dimension. In a separate experiment, the experimenter presents a contrast pattern within a wedge that rotates around fixation. This stimulus elicits responses that are specific to certain angles and these responses define the angle dimension. Together, the ring and wedge measurements determine the most effective visual field position for each voxel.

The images in Figure 1 show fMRI eccentricity and angle maps in the most posterior portion of occipital cortex. The color overlay specifies angle on the left mesh and eccentricity on the right mesh. There is a single, integrated eccentricity map near the occipital pole. A great deal of the cortical surface area at the pole represents the fovea, and there is a systematic shift toward more peripheral representations in the posterior-to-anterior direction. The integrated eccentricity representation includes V1, V2, V3 and hV4, although the hV4 part of the map is a bit compressed. Based on the eccentricity data alone, one would have no basis for segregating the activated cortex into different regions.

The segregation into multiple maps becomes clear from examining the angle representations. The V1 map has a continuous angle representation of the contralateral visual field, spanning the lower vertical meridian (green in the pseudocolor map) to the upper vertical meridian (red). The angle representation reverses at the vertical meridians, and this marks the boundary with V2. The V1 map is surrounded by a dorsal and ventral section of V2, which represent the lower (green-cyan) and upper (red-blue) visual field. The V2 map is, in turn, surrounded by dorsal and ventral sections of V3. This nested organization for V1-V3 is typical of non-human primates. But the confirmation that this organization is present in human was only made in the early 1990s by a combination of neurology and fMRI (20, 21, 23-25).

Visual stimuli elicit activity in about twenty percent of the human brain, covering the entire occipital lobe and extending into portions of temporal and parietal cortex (26). It is likely that occipital cortex is completely covered by maps, though some regions have proven difficult to measure (15). Identifying the organization within human visual cortex is essential for interpreting fMRI data from visual cortex and for building meaningful computational theories of vision. This project has had excellent progress. Measurements like those in Figure 1 show that the general spatial layout of early human visual maps - V1, V2, and V3 - is similar to non-human primate. However, research has revealed substantial differences in the size, spatial layout and responsiveness between human and non-human primate extrastriate maps (e.g., V3, hV4, V3A/B, VO-1). These findings have been reviewed recently, and we refer the reader to those reviews to learn more about this work (27-29).

## Stimulus-referred measurements

It is worthwhile to step back and consider what exactly is measured when a visual field map is defined: the map specifies which stimulus position most effectively drives the response at each cortical location. Thus, the map characterizes cortex in terms of the stimulus. Such *stimulus-referred* (also called input-referred) descriptions of neural responses play a key role in vision science. The great majority of visual neuroscience measurements use a stimulus-referred approach to characterize neural responses.

Receptive field measurement is a classic and particularly clear example (30). Suppose one measures the response of a V1 neuron to a small spot presented at different locations in the

visual field. The cell will respond when the spot is within a small region of the visual field, and this region is called the receptive field (RF). Note that the RF is a description of the stimulus properties (locations) that evoke a response. There is no description of the proximal inputs to the cell - lateral geniculate neurons, other V1 neurons, feedback signals from extrastriate cortex, and inputs received from the pulvinar. Stimulus-referred descriptions are a theoretical construct; a V1 neuron lives and dies in the dark, never being directly stimulated by photons. In describing the RF of a cell, the optical components of the eye and the extensive neural and glial network that gives rise to the RF are not explicitly characterized.

Stimulus-referred descriptions can be applied to many properties in addition to visual field position, such as orientation, direction, and wavelength (31). Stimulus-referred measurements summarize neural circuit responses without requiring the construction of a circuit model. This capability is important because such circuit models are presently beyond the reach of neuroscience methods.

Perhaps the most valuable aspect of stimulus-referred measurement is that it supports the coordination of insights from many parts of vision science - including optics, retinal processing, cortical circuitry, local field potentials, scalp recordings, and perception. Integration across these measures is challenging because each samples the nervous system in its own way and produces outputs with different units. For example, microelectrodes measure voltages or spike rates, calcium imaging measures photons, fMRI measures modulation in blood oxygenation, and perception measures subject reports. The stimulus is a unifying framework for vision science; the stimulus representation serves as a common ground where results from very different measures are compared.

The use of stimulus-referred measurements is very common in vision science, just as input-referred measurements are very common in engineering (31). They are so ubiquitous that the beauty and value of the approach is rarely taught. One objective of this chapter is to make the idea and its value explicit.

## **Population receptive field models**

The success in the parcellation of visual cortex into maps provides a foundation for a new phase of investigation: building computational models of fMRI responses to visual stimuli. The goal of this work is to precisely express and test neural processing principles. Stimulus-referred computational models offer the best hope for coordinating different types of visual measures into a unified theory. This new phase of modeling could not take place without the first phase. Response properties differ across maps; interpreting the measurements is problematic unless one knows which map is the source of the measurement.

In an early step towards theory, Tootell et al. (32) observed that reducing the width of a contrast pattern, such as an expanding ring contrast pattern, substantially reduced the duration of the V1 on-response but had little effect on the V3A on-response. They explained the difference by the

hypothesis that V3A receptive fields cover more of the visual field than V1 receptive fields. Qualitatively, the on-response in V1 was governed by the stimulus width but in V3A the on-response was governed by the receptive field width. Smith et al. (33) systematically investigated this idea, quantifying the proportion of the time that the fMRI response is elevated compared to baseline (the duty cycle) as thin rings or wedges traversed the visual field. The duty cycle differs substantially between cortical locations, and they explained these differences in terms of the size of the receptive field of neurons in each cortical location.

## **Construction of a linear population receptive field (pRF) model**

Dumoulin and Wandell (34) built upon the prior work in several ways. First, they defined an explicit computational model to predict the fMRI response at each voxel. The key element of the model is the concept of the population receptive field (pRF), named by Victor et al. (35) who used the approach in local field potential measurements in macaque. The pRF summarizes the collective receptive fields of all the cells giving rise to the response within a voxel.

The initial models approximated the pRF by a two-dimensional Gaussian, characterized by a center position,  $(x,y)$ , and spread  $(\sigma)$ . These parameters are specified in the visual field relative to the gaze location (fixation). By using a stimulus-referred description, Smith et al. (33) and Dumoulin and Wandell (34) were able to compare fMRI measurements with data obtained using other brain measurement methods. For example, the pRF spread measured using fMRI could be plotted against the single-unit receptive field size measured using macaque electrophysiology.

Second, Dumoulin and Wandell implemented a computational model of the fMRI time series. A model of the fMRI time series is possible in visual cortex because the response amplitude in individual subjects is large and there is no need to average across subjects. Implementing a full model provides the investigator with an opportunity to predict fMRI time series to different types of stimuli. Dumoulin and Wandell took advantage of the model implementation to measure maps using a new type of stimulus. The model also made possible the quantification of a new stimulus feature (pRF size) within maps.

Figure 2 shows a pRF analysis tool, implemented by Rory Sayres, that several groups have used to examine and interpret fMRI time series. The three panels show responses and analyses for voxels in V1, V2 and V3A. The stimulus was a set of oriented bars that moved slowly across in the visual field along eight different trajectories. Occasionally, the bars were removed so that the observer simply viewed a zero contrast field (34). The estimated pRF and the predicted and measured time series responses are shown for each voxel. Plainly, the predicted time series are in good agreement with the measurements. The estimated pRF sizes differ substantially across maps, confirming the prior work.

## **What does a pRF measure?**

Human cortex contains 50,000 neurons per  $\text{mm}^3$  so that a typical 2 mm isotropic voxel contains about 400,000 neurons (36); the 1 mm isotropic voxels depicted in Figure 2 contain about

50,000 neurons each. A subset of these neurons, as well as the local glial cells, respond to any given stimulus, and it is this population response that determines the voxel's receptive field. Furthermore, pRF parameters will depend on the specific population of neurons stimulated by the pattern that defines the texture within the moving bar. Features such as the temporal frequency, wavelength composition, and so on may excite different populations and influence the pRF parameters.

The RF measured using single-unit physiology has a related theoretical status. Each neuron in V1 is contacted by about 10,000 other neurons, and cells in their neighborhood in turn contact these neurons. When a small point is presented in the visual field, voltage sensitive dye measurements show that activity in the superficial layers of cortex spreads over a distance of several millimeters, commensurate with the size of an fMRI voxel (37). Hence, the receptive field measured in a single V1 cell in layers 2/3 reflects the pooled activity of its inputs and its role in the neural circuit.

The principal difference between the single-unit RF and the pRF is that the RF measurements taps into the circuit activity at a single point within the neural plexus, while the pRF is a mean-field measurement of the circuit activity. The key limitation of mean-field fMRI measurements is obvious - spatial resolution. However, an advantage is that fMRI measurements provide a much larger field of view and can reveal coordinated activity in remote sites. The fMRI measurement is also sensitive to signals that are missed by single unit RF measurements. In some cases where BOLD and single unit measurements diverge, the BOLD signal correlates best with perceptual judgments (38). The BOLD signal is also sensitive to glial responses (39), a cell class often neglected in electrophysiological measurements in animals. Finally, fMRI provides direct information about human, while single-unit physiology is carried out in animal models whose circuits may differ.



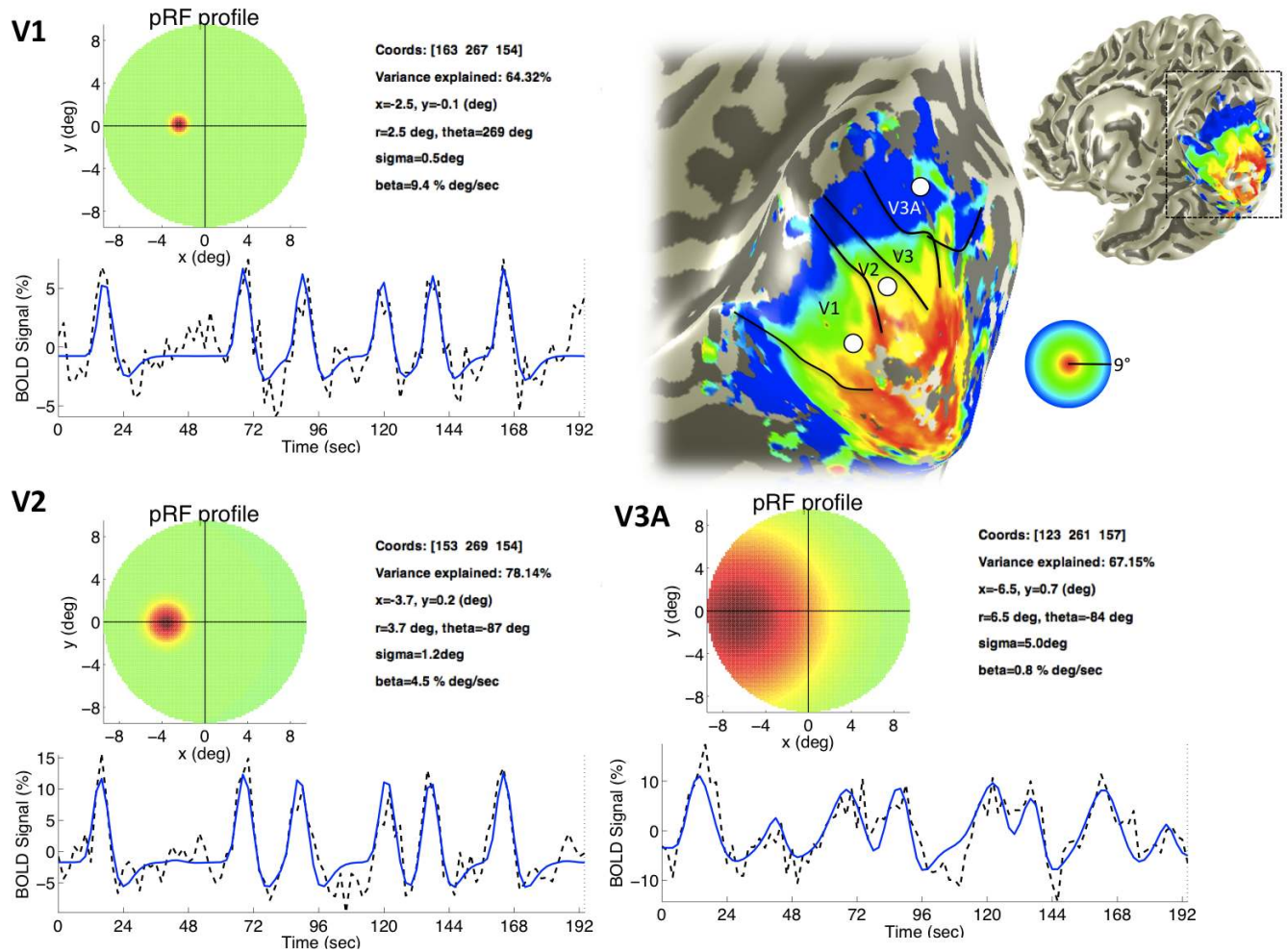


**Figure 2. A tool to analyze the population receptive field (pRF).** The fMRI time series were measured with a 7 Tesla scanner at a resolution of  $1 \text{ mm}^3$  voxels. The stimulus was a contrast pattern within a slowly translating bar aperture. The aperture swept through the visual field at different angles; occasionally the contrast pattern was turned off. The three plots show the fMRI signal measured at voxels located in three different locations (white circles in V1, V2 and V3A; upper right image). The dashed black lines are measurements and the solid blue lines are pRF model fits. The estimated pRF for each voxel is shown in the image panels. The three time series responses to the same pattern differ in timing and width. This time series difference is modeled by the center position and size of the pRF. The tool is part of the open source vistasoft package (<http://github.com/vistalab>). Data obtained in collaboration with E. Yacoub and K. Ugurbil.

The pRF framework has been applied usefully in a number of studies. For example, the framework has been used to clarify certain visual field maps (10, 15, 40) and to compare pRF sizes between controls and subjects with neurological conditions (41, 42). The method has been applied to measure plasticity (43) and the effect of task-demands (44). It has been used in

fMRI studies of visual cortex in animal models (45, 46) and to elucidate the relationship with anatomy (47).

## Improving the linear pRF model

It is a truism that all models are wrong, but some are useful (48). The first pRF models are useful, but they are inaccurate in several ways. Our group and others continue to work to identify and reduce the model deficiencies (49-51)

The model failures become apparent when we use the pRF model to predict the fMRI time series response to a larger range of visual stimuli. Returning to the original measurements by Tootell et al. (32), Winawer set out to use the pRF model to predict responses to both thin and thick bars. It became apparent that the Dumoulin and Wandell pRF model could not account for even such a modest increase in the range of stimuli.

Kay et al. (52) show that the failure arises from a basic assumption: linear summation of the contrast across the spatial receptive field. The failure of spatial linearity can be measured in a simple experiment (Figure 3). Consider a voxel that responds to contrast near the horizontal midline. We can present a stimulus that fills either the upper half of the pRF or the lower half. If spatial linearity holds, the response to a stimulus that fills both the upper and lower portions of the pRF should equal the sum of the responses to upper and lower separately. This spatial summation prediction is somewhat inaccurate in the posterior maps, V1 and V2, and it misses substantially in anterior extrastriate maps (52). Kay et al. showed that incorporating a static nonlinearity into the standard pRF model can remedy the failure of spatial linearity. Furthermore, Kay et al. show that the specific form of the non-linearity fit to the BOLD signal is compatible with existing models of single neuron spike rates, such as divisive normalization (53). Connecting these two very different kinds of measurements, fMRI and single unit spiking, is possible because stimulus-referred models are fit in both domains<sup>1</sup>.

In a separate study, Kay et al. (55) further extended the modeling effort by developing a new pRF model that accounts for measurements of responses to an even wider range of stimuli. The new model is also distributed as a full computation (<http://kendrickkay.net/socmodel/>). This model is much more complex than the Dumoulin and Wandell formulation, allowing it to predict the responses to a much wider range of stimuli.

---

<sup>1</sup> It is tempting to think of divisive normalization as a circuit model rather than a stimulus-referred model because there has been substantial work trying to explain normalization in terms of circuit properties such as shunting inhibition, resistance and capacitance (54. Ferster D (2010) Diverse mechanisms of contrast normalization in primary visual cortex. *Journal of Vision* 10(15):29). But in fact divisive normalization model parameters are specified in the stimulus domain, including contrast and orientation. In fact, the circuits giving rise to normalization are largely unknown (53. Carandini M & Heeger DJ (2012) Normalization as a canonical neural computation. *Nat Rev Neurosci* 13(1):51-62). Normalization, like linear filtering, is an application of the stimulus-referred approach.

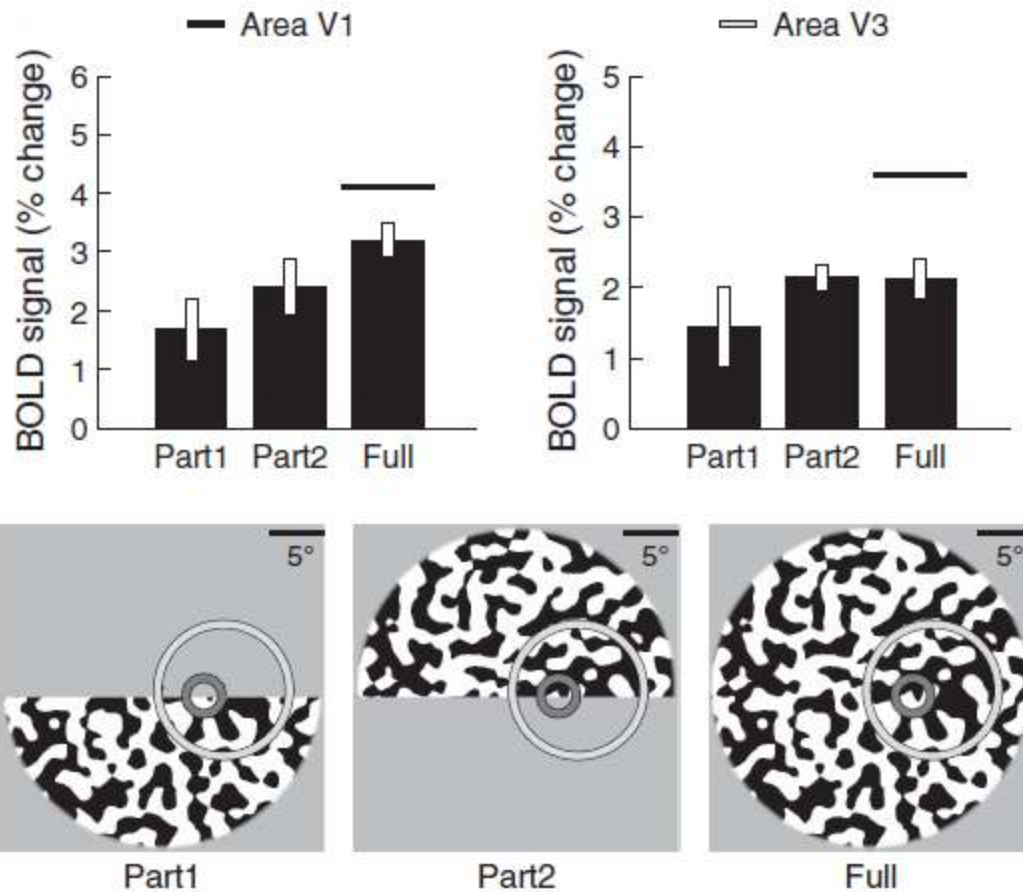


**Figure 3 Spatial summation of contrast fails to predict the fMRI signal in human visual cortex.** The upper bar plots show the measured responses to a lower field stimulus, an upper field stimulus, and the combination of the two. For the voxel in V1 (upper left) and V3 (upper right), the response to the full aperture is less than the sum of the responses to the two partial apertures, and hence less than the linear prediction (indicated by the black lines). The failure of linearity is more severe for V3 than for V1. The lower images show the 2- $\sigma$  circle for the pRF for the two voxels (dark line V1; light line V3). After Kay et al. (52).

## Integration of fMRI and ECoG data

There has been remarkable progress in inventing new ways to measure neural signals. Modern methods range from well-isolated single units to local field potentials, calcium imaging, voltage sensitive dyes, and intrinsic functional measures such as fMRI. These methods provide different types of information about the circuitry, and there is much to be gained by understanding how to combine insights from different methods (56-58).

The stimulus-referred measurement approach integrates the diverse measures made by visual neuroscientists. In a recent study we measured population receptive fields using both ECoG

and fMRI, and we asked whether the two data sets might be explained by the same pRF model. The ECoG data are a voltage time series captured at millisecond resolution, while the fMRI signal is a modulation in the local oxygenation sampled every second or two. By using stimulus-referred measurements, we can compare the measurements in a common reference frame, bypassing the problem of incommensurate units.

There were several straightforward findings (Figure 4). First, the ECoG signal contains responses from at least two neural sources, broadband and stimulus-locked, and we created accurate pRF models of each response component. Second, the receptive field position and size derived from the ECoG and the fMRI responses agreed. Third, the spatial summation properties of broadband, but not stimulus-locked, ECoG signals match the spatial summation measured in the fMRI signal. From this stimulus-referred analysis we concluded that the fMRI signal arises principally from the broadband ECoG component.

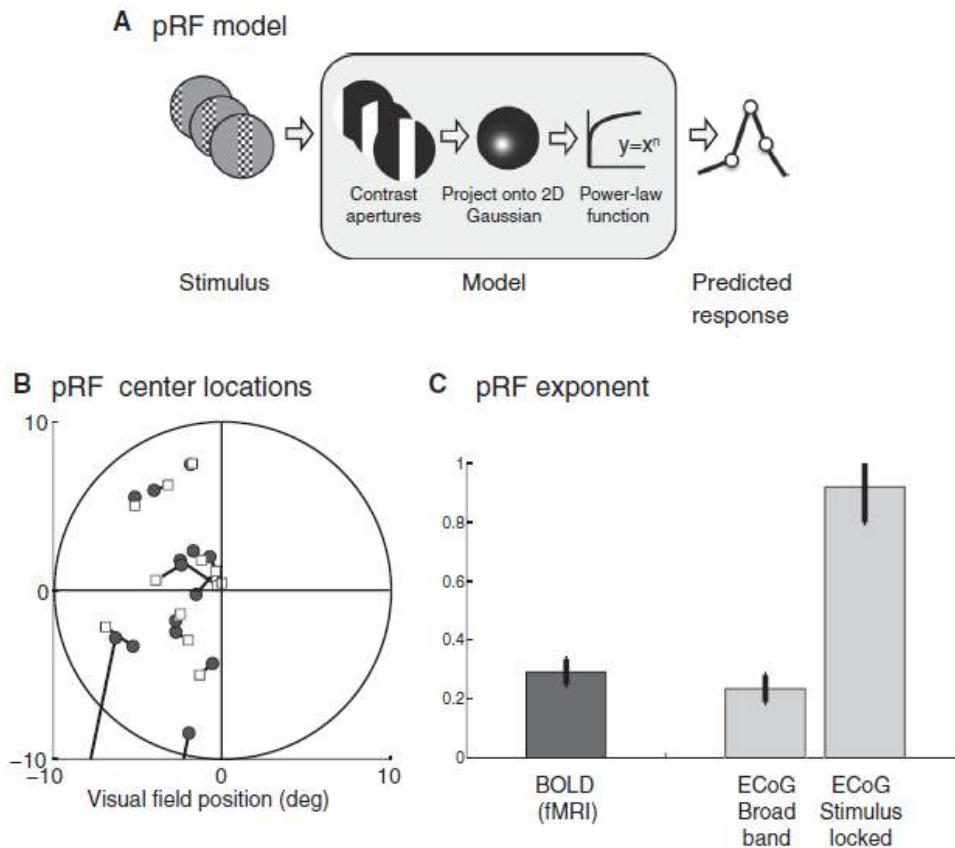


**Figure 4. Stimulus-referred models integrate different measurement modalities.** (A) A stimulus-referred pRF model (52) was applied to V1, V2 and V3 responses from retinotopic stimuli. Measurements were obtained using both ECoG and fMRI, and we further separated the ECoG signal into two components - an asynchronous broadband signal that measured a stimulus-driven increase in response variance, and a stimulus-locked response that modulated in synchrony with each contrast reversal. The CSS model fit the measured time series of all three signals. (B) The estimated pRF centers

to the two types of ECoG are similar (filled and open signals; lines connect estimates from a single electrode). These pRF centers also match the expected visual field map from fMRI (not shown). (C) The estimated spatial summation exponent,  $n$ , from the pRF model is highly compressive ( $n < 1$ ) for fMRI and for ECoG broadband responses. The exponent is close to linear ( $n \sim 1$ ) for the stimulus-locked response. Hence, fMRI spatial summation matches broadband ECoG, but not stimulus-locked ECoG. After Winawer et al. (59). See also (60) for a stimulus-referred approach to understanding the relationship between ECoG and fMRI pRF measurements.

## Discussion

As computational models of vision increase in accuracy and power (i.e. account for a larger range of stimuli), they become more complex. The original Tootell et al. and Smith et al. papers could reason correctly and informally about receptive field sizes. But they accounted for very few stimuli and relied on summary measures of the response time series. Modern computational models that account for a much larger range of stimuli and predict the full time series are significantly more complex (Figure 5). These models are not captured in a small set of formulae, and it is necessary to use software implementations to generate predictions.

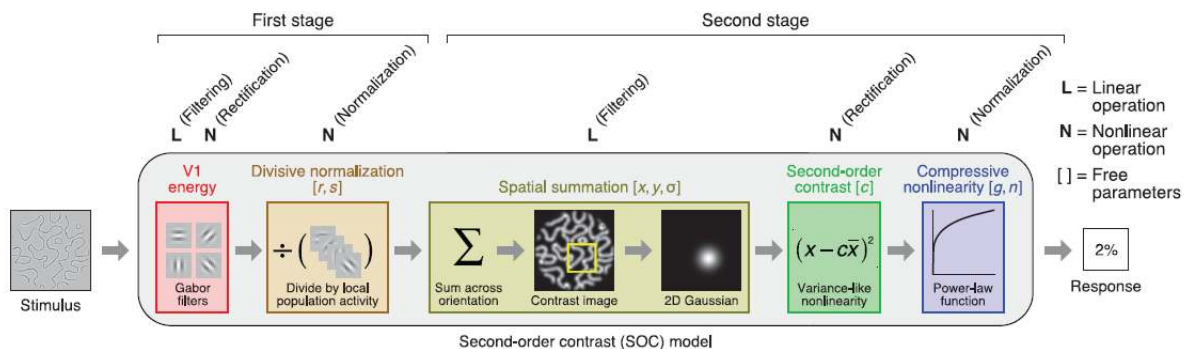


**Figure 5. A modern computational model of fMRI signals in visual cortex.** The model developed by Kay et al. integrates an array of widely used visual neuroscience computations (energy, divisive normalization, spatial summation, second-order contrast, compressive nonlinearity). These operations are organized into two stages of sequential linear, nonlinear, nonlinear (LNN) operations. To develop models of this complexity - which are surely much simpler than what will ultimately be required - requires software implementations and the ability to test different forms of the model on multiple classes of stimuli. After Kay et al. (55).

Computational modeling is a cumulative process that expands the domain of application by accounting for an increasing range of experimental conditions. This differs from experimental work focused on hypothesis testing. Computational models are built by testing new features while always checking for the impact of the new features on previous predictions; new data are

not viewed as a hypothesis test that results in accepting or rejecting the model by a statistical test. Rather, computational model development is a process yields increasingly refined predictions from a sustained effort; we believe this is one of its great benefits.

Finally, we note that even if a computational model is imperfect, it can still be useful. For example, it is reasonable to use linear pRF models to estimate receptive field center positions when using a single bar width, even though the model does not generalize to multiple bar widths. The use of a model that is adequate for a given objective is common in other branches of science and engineering. After all, we do not calculate local travel time using relativity and the Earth's curvature.

## **Which brain measurements are best?**

We have emphasized the value of stimulus-referred models for integrating data from different types of measurements. We are aware that an alternative scientific approach is to deny the validity of all but one measure:

Any analysis of plastic reorganization at a neuronal locus needs a veridical measure of changes in the functional output — that is, spiking responses of the neurons in question. (61).

We think it is best to be open to the value of many measurement methods. In fact, we don't think there is a strong alternative to this approach because it is illusory to think that even within a measurement domain the signals form a single, unitary class. For example, in the retina the same stimulus produces different responses in different cell types, such as retinal ganglion cells of the parasol and midget classes. The voltage response in the ECoG signal arises from multiple sources with distinct properties. In cortex some spikes are relevant for only local calculations, while others are communicated by long-range projections to other cortical regions. Thus, it is incorrect to expect that the fMRI response or a perceptual judgment will match "spiking responses" when there are so many different types of neurons and so many different types of spikes.

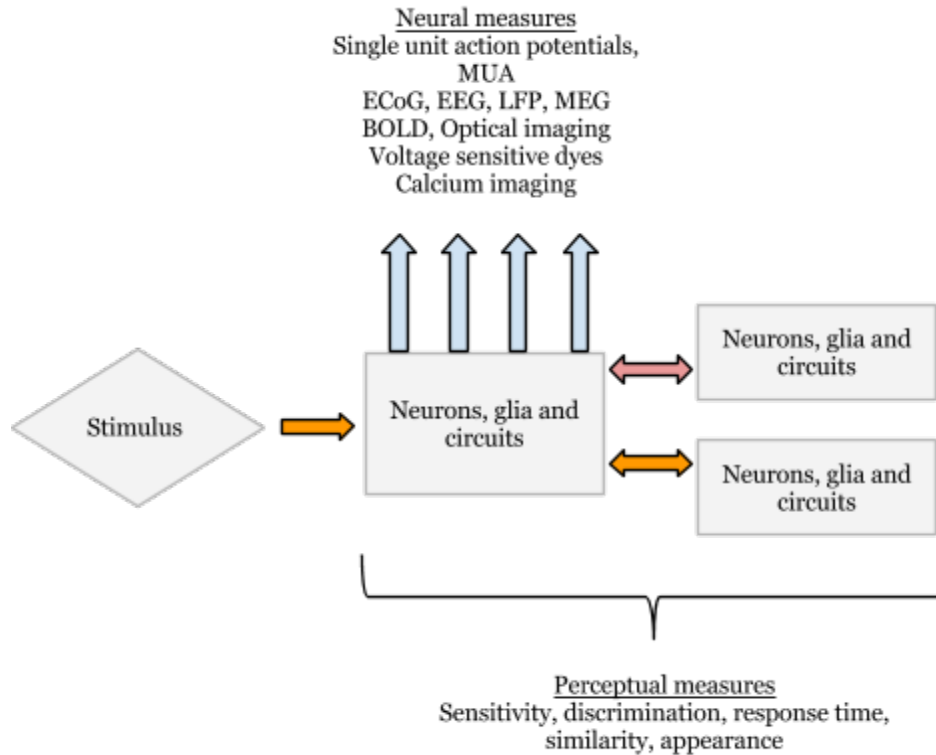


**Figure 6. An integrative view of modeling visual brain function.** Computational models of visual neuroscience must take a broad view that spans the stimulus, brain systems, and perceptual measures. Because visual responses arise from a well-characterized physical stimulus, we can use stimulus-referred theories. Computational models and stimulus-referred measurements provide a rigorous means for integrating information about neurons, glia and circuits, as well as the instruments and many types of perceptual measures.

Further, the modern neuroscientist should consider the likelihood that cortical function depends importantly on several types of cells. There are many reasons to believe that responses in other brain cells, such as the many types of glia present in the human brain, are important for brain function (62). If the fMRI signal informs us about these responses as well as neuronal responses, should we complain? Or should we be grateful to have this additional information?

We advocate for an integrative view of the visual system (Figure 6). We suggest that a goal of visual neuroscience is to develop models that begin with a careful description of the stimulus, integrate experimental observations derived from multiple measures of brain activity and circuitry, model these multiple types of responses, and rigorously understand the relationship between certain aspects of the brain activity and perception.

## References

1. Phillips CG, Zeki S, & Barlow HB (1984) Localization of function in the cerebral cortex. Past, present and future. *Brain* 107(Pt 1):327-361.
2. Munk H (1879) Weitere zur Physiologie der Sehsphäre der Grosshirnrinde. *Verhandlungen der Physiologischen Gesellschaft zu Berlin*:581–594.
3. Zeki S (1993) *A Vision of the Brain* (Blackwell Scientific Publications, London).
4. Inouye T (1909) *Die Sehstörungen bei Schussverletzungen der kortikalen Sehsphäre* (W. Engelmann, Leipzig, Germany).
5. Henschen SE (1893) On the visual path and centre. *Brain* 16:170–180.
6. Holmes G (1918) Disturbances of vision by cerebral lesions. *British Journal of Ophthalmology* 2:353-384.
7. Holmes G & Lister WT (1916) Disturbances of vision from cerebral lesions, with special reference to the cortical representation of the macula. *Brain* 39:34 - 73.
8. Hubel DH & Wiesel TN (1977) Ferrier lecture. Functional architecture of macaque monkey visual cortex. *Proc R Soc Lond B Biol Sci* 198(1130):1-59.
9. Felleman DJ & Essen DCV (1991) Distributed hierarchical processing in the primate cerebral cortex. *Cerebral Cortex* 1:1-47.
10. Arcaro MJ, McMains SA, Singer BD, & Kastner S (2009) Retinotopic organization of human ventral visual cortex. *J Neurosci* 29(34):10638-10652.
11. Dechent P & Frahm J (2003) Characterization of the human visual V6 complex by functional magnetic resonance imaging. *Eur J Neurosci* 17(10):2201-2211.
12. Kolster H, Peeters R, & Orban GA (2010) The retinotopic organization of the human middle temporal area MT/V5 and its cortical neighbors. *J Neurosci* 30(29):9801-9820.
13. Sereno MI, Pitzalis S, & Martinez A (2001) Mapping of contralateral space in retinotopic coordinates by a parietal cortical area in humans. *Science* 294(5545):1350-1354.
14. Konen CS & Kastner S (2008) Representation of eye movements and stimulus motion in topographically organized areas of human posterior parietal cortex. *J Neurosci* 28(33):8361-8375.
15. Winawer J, Horiguchi H, Sayres RA, Amano K, & Wandell BA (2010) Mapping hV4 and ventral occipital cortex: the venous eclipse. *J Vis* 10.
16. Ogawa S, *et al.* (1992) Intrinsic signal changes accompanying sensory stimulation: Functional brain mapping with magnetic resonance imaging. *Proc. Nat. Acad. Sci* 89:591-5955.
17. Kwong KK, *et al.* (1992) Dynamic magnetic resonance imaging of human brain activity during primary sensory stimulation. *Proc.Natl.Acad.Sci.USA* 89(12):5675-5679.
18. Engel SA, *et al.* (1994) fMRI of human visual cortex. *Nature* 369(6481):525.
19. DeYoe EA, Bandettini P, Neitz J, Miller D, & Winans P (1994) Functional magnetic resonance imaging (fMRI) of the human brain. *J Neurosci Methods* 54(2):171-187.
20. Sereno MI, *et al.* (1995) Borders of multiple human visual areas in humans revealed by functional mri. *Science* 268:889-893.
21. Engel SA, Glover GH, & Wandell BA (1997) Retinotopic organization in human visual cortex and the spatial precision of functional MRI. *Cereb Cortex* 7(2):181-192.
22. Warnking J, *et al.* (2002) fMRI retinotopic mapping--step by step. *Neuroimage* 17(4):1665-1683.
23. Horton JC & Hoyt WF (1991) Quadrantic visual field defects: a hallmark of lesions in extrastriate (V2/V3) cortex. *Brain* 114:1703-1718.



24. Horton JC & Hoyt WF (1991) The representation of the visual field in human striate cortex. A revision of the classic Holmes map. *Arch Ophthalmol* 109(6):816-824.
25. DeYoe EA, *et al.* (1996) Mapping striate and extrastriate visual areas in human cerebral cortex. *Proc. Natl. Acad. Sci. (USA)* 93:2382-2386.
26. Wandell BA, Dumoulin SO, & Brewer AA (2009) Visual Cortex in Humans. *Encyclopedia of Neuroscience*, ed Squire L (Elsevier).
27. Silver MA & Kastner S (2009) Topographic maps in human frontal and parietal cortex. *Trends Cogn Sci* 13(11):488-495.
28. Wandell BA, Dumoulin SO, & Brewer AA (2007) Visual field maps in human cortex. *Neuron* 56(2):366-383.
29. Wandell BA & Winawer J (2011) Imaging retinotopic maps in the human brain. *Vision Res* 51(7):718-737.
30. Hartline HK (1938) The response of single optic nerve fibers of the vertebrate eye to illumination of the retina. *Am J. Physiol.* 121:400-415.
31. Wandell BA (1995) *Foundations of Vision* (Sinauer Press, Sunderland, MA).
32. Tootell RB, *et al.* (1997) Functional analysis of V3A and related areas in human visual cortex. *J Neurosci* 17(18):7060-7078.
33. Smith AT, Singh KD, Williams AL, & Greenlee MW (2001) Estimating receptive field size from fMRI data in human striate and extrastriate visual cortex. *Cereb Cortex* 11(12):1182-1190.
34. Dumoulin SO & Wandell BA (2008) Population receptive field estimates in human visual cortex. *Neuroimage* 39(2):647-660.
35. Victor JD, Purpura K, Katz E, & Mao B (1994) Population encoding of spatial frequency, orientation, and color in macaque V1. *J Neurophysiol* 72(5):2151-2166.
36. Braitenberg V & Schüz A (1998) *Cortex: Statistics and Geometry of Neuronal Connectivity* 2nd Ed.
37. Grinvald A, Lieke EE, Frostig RD, & Hildesheim R (1994) Cortical point-spread function and long-range lateral interactions revealed by real-time optical imaging of macaque monkey primary visual cortex. *J. Neurosci.* 14:2545-2568.
38. Maier A, *et al.* (2008) Divergence of fMRI and neural signals in V1 during perceptual suppression in the awake monkey. *Nat Neurosci* 11(10):1193-1200.
39. Schulz K, *et al.* (2012) Simultaneous BOLD fMRI and fiber-optic calcium recording in rat neocortex. *Nat Methods* 9(6):597-602.
40. Amano K, Wandell BA, & Dumoulin SO (2009) Visual field maps, population receptive field sizes, and visual field coverage in the human MT+ complex. *J Neurophysiol* 102(5):2704-2718.
41. Levin N, Dumoulin SO, Winawer J, Dougherty RF, & Wandell BA (2010) Cortical maps and white matter tracts following long period of visual deprivation and retinal image restoration. *Neuron* 65(1):21-31.
42. Hoffmann MB, *et al.* (2012) Plasticity and stability of the visual system in human achiasma. *Neuron* 75(3):393-401.
43. Brewer AA, Barton B, & Lin L (2012) Functional plasticity in human parietal visual field map clusters: Adapting to reversed visual input. *Journal of Vision* 12(9):1398-1398.
44. de Haas B, Schwarzkopf DS, Anderson EJ, & Rees G (2013) Effects of perceptual load on population receptive fields. *Journal of Vision* 13(9):290-290.
45. Smirnakis SM, Keliris G, Shao Y, Papanikolaou A, & Logothetis N (2012) Population receptive field measurements in macaque visual cortex. *Journal of Vision* 12(9):1397-1397.
46. Shao Y, *et al.* (2013) Visual cortex organisation in a macaque monkey with macular degeneration. *European Journal of Neuroscience*.

47. Benson NC, Butt OH, Jain S, Brainard DH, & Aguirre GK (2013) Cortical surface structure predicts extrastriate retinotopic function. *Journal of Vision* 13(9):271-271.
48. Box G & Draper N (1987) *Empirical model-building and response surfaces* (Wiley, New York).
49. Binda P, Thomas JM, Boynton GM, & Fine I (2013) Minimizing biases in estimating the reorganization of human visual areas with BOLD retinotopic mapping. *Journal of Vision* 13(7).
50. Alvarez I, De Haas B, Clark CA, Rees G, & Schwarzkopf DS (2013) Optimal stimulation for population receptive field mapping in human fMRI. *Journal of Vision* 13(9):31-31.
51. Zuiderbaan W, Harvey BM, & Dumoulin SO (2012) Modeling center-surround configurations in population receptive fields using fMRI. *J Vis* 12(3):10.
52. Kay K, Winawer J, Mezer A, & Wandell BA (2013) Compressive spatial summation in human visual cortex. *Journal of neurophysiology*.
53. Carandini M & Heeger DJ (2012) Normalization as a canonical neural computation. *Nat Rev Neurosci* 13(1):51-62.
54. Ferster D (2010) Diverse mechanisms of contrast normalization in primary visual cortex. *Journal of Vision* 10(15):29.
55. Kay KN, Winawer J, Rokem A, Mezer A, & Wandell BA (2013) A Two-Stage Cascade Model of BOLD Responses in Human Visual Cortex. *PLoS computational biology* 9(5):e1003079.
56. Goense J & Logothetis NK (2008) Neurophysiology of the BOLD fMRI signal in awake monkeys. *Current Biology* 18(9):631-640.
57. Niessing J, *et al.* (2005) Hemodynamic signals correlate tightly with synchronized gamma oscillations. *Science* 309(5736):948-951.
58. Mukamel R, *et al.* (2005) Coupling between neuronal firing, field potentials, and fMRI in human auditory cortex. *Science* 309(5736):951-954.
59. Winawer J, *et al.* (2013) Asynchronous Broadband Signals Are the Principal Source of the BOLD Response in Human Visual Cortex. *Current Biology*.
60. Harvey BM, *et al.* (2013) Frequency specific spatial interactions in human electrocorticography: V1 alpha oscillations reflect surround suppression. *Neuroimage* 65:424-432.
61. Calford MB, *et al.* (2005) Neuroscience: rewiring the adult brain. *Nature* 438(7065):E3; discussion E3-4.
62. Bullock TH, *et al.* (2005) Neuroscience. The neuron doctrine, redux. *Science* 310(5749):791-793.